Numerical Simulation of Residual Stress and Deformation Considering Phase Transformation Effect†

DENG Dean*, LUO Yu**, SERIZAWA Hisashi ***, SHIBAHARA Masakazu **** and MURAKAWA Hidekazu *****

Abstract

The objective of this work was to investigate the effects of solid-state phase transformation on residual stresses and deformations in low carbon and medium carbon steels welded by the tungsten inert gas (TIG) arc welding process. An uncoupled thermal-mechanical three-dimensional finite element model that took into account the solid-state phase transformation was developed. In this study, different continuous cooling transformation (CCT) diagrams were used to predict the fractions of martensite for the coarse-grained HAZ and the fine-grained HAZ, respectively. Effects of volume change due to austenite-martensite transformation on residual stress and distortions were studied. The analysis of low carbon steel revealed that the residual stress and deformation did not seem to be affected by phase transformation during cooling. However, for medium carbon steel, the residual stresses and deformation were significantly affected by low temperature phase transformation..

KEY WORDS: (Finite element method) (Welding residual stress) (Welding deformation) (Phase transformation) (Tungsten inert gas arc welding)

1. Introduction

One of the major problems in welded structures is the welding residual stress and the distortion due to local heating, Residual stresses that develop in and around the welding zone are detrimental to the integrity and the service behavior of welded structures. The welding residual stress may promote brittle fracture, reduce the buckling strength and the fatigue life and promote stress corrosion cracking during service. Residual tensile stress also promotes cold cracking associated with hydrogen in certain steels before the welded part is put into service[1]. Welding distortion often results in problems such as dimensional inaccuracies during assembly and cost increase of the product.

Several factors may contribute to the formations of residual stress and deformation. The plastic deformation produced in the base metal is a function of structural, material, and fabrication parameters. The structural parameters include the joint type and the thickness of plates. The material parameters reflect the metallurgical condition of base metal and the weld metal. Fabrication parameters include the welding method, heat input, preheating, welding sequence and the restraint condition.

In certain steel welded parts, the solid-state austenite-martenite transformation during cooling has a significant influence on the residual stresses and distortion [2]. The martensite transformation is a diffusionless solid-state shear deformation[3]. In steels, martensite is formed from austenite containing carbon atoms and, in view of the diffusionless nature of its formation, ideally inherits the carbon atoms of the parent austenite. The carbon atoms are trapped in octahedral interstitial sites between iron atoms, producing a body centered tetragonal (bct) structure, and are in super-saturation relative to the body centered cubic (bcc) ferrite. In addition to the fact that the chemical composition of the austenite is directly inherited by the martensite, the martensitic shear deformation is accomplished by a plain-strain shape change parallel to a set of crystallographic planes of the parent austenite. Therefore, when the martensite is formed, the volume of metal is increased, and the transformation plasticity is also produced. During the welding process, the magnitude of the volumetric expansion at the heat-affected zone (HAZ) and the fusion zone (FZ) depends upon the volume fraction of martensite that formed.

Accurate prediction and reduction of welding

† R eceived on December 1, 2003

*Foreign Research Fellow (Chongqing university, China)
**Associate Professor (Shanghai Jiaotong university, China)
***Associate Professor
****Research Associate, Kanazawa Institute of Technology
*****Professor

Transactions of JWRI is published by Joining and Welding Research Institute of Osaka University, Ibaraki, Osaka 567-0047, Japan

residual stress and deformation are critical in improving the quality of the weldments. To evaluate residual stress and deformation accurately, metallurgical phase transformation must be considered. In the present study, a FE method considering solid-state phase transformation has been developed based on the existing researches [1-5], and the effectiveness of the proposed numerical method for analyzing the residual stress and the distortion specific to tungsten inert gas (TIG) arc welding is demonstrated. The finite element analysis package ABAQUS [6] was used in this study.

2. Finite Element Modelling

The evolution of the residual stresses and distortion are investigated by means of finite element method. In order to accurately capture the residual stress and distortion in the welded plate, a three-dimensional finite element model was developed. The thermo-mechanical behavior of the weldment during welding was simulated using uncoupled formulation, because the dimensional changes in welding are negligible and mechanical work done is insignificant compared to the thermal energy from the welding arc.

The heat conduction problem is solved independently from the stress problem and phase state to obtain temperature history. However, the formulation considers the contributions of the transient temperature field to the stress analysis through thermal expansion, as well as temperature-dependent thermo-physical and mechanical properties. The solution procedure consists of two steps. First, the temperature distribution and its history in the welding model is computed by the heat conduction analysis. The temperature history is employed as a thermal load in the subsequent mechanical elastic plastic calculation of the residual stress field. In this step, the volume fraction of martensite is also calculated, and volume change due to phase transformation is considered through modifying the thermal expansion coefficient over the temperature range in which austenite changes into martensite.

2.1 Heat Source and Thermal Analysis

In this study, a plate model as shown in **Fig. 1** was used. Because of the symmetry, one half of the model was selected as the analysis model. The FE model is shown in **Fig. 2** with 4000 brick elements and 5355 nodes. It has a fine grid in the welding zone. The length, the width and the thickness of the model are 200mm, 100mm and 6mm, respectively.

Tungsten inert gas (TIG) arc welding is the most frequently modelled arc-welding process in which the heat source is a non-consumable electrode. In the direct current electrode negative TIG process, the weldments are joined together by the following four primary mechanisms (1) Kinetic energy of the electrons that constitute the arc current, (2) Heat of condensation of the electrons penetrating the solid work surface, (3) Radiation from the arc, (4) Thermal conduction from the arc plasma to work-piece. The first two mechanisms constitute the major source of energy for the weldment [7].

According to the nature in which energy is transferred from the arc, the heat input of the TIG arc welding process to the weldment can be modelled by a point source or a line source. A more realistic approach is to consider the heat flux on the surface or the heat generation distribution in the metal, or a combination of the two.

In this work, the heat from the moving welding arc was applied as a volumetric heat source with a double ellipsoidal distribution proposed by Goldak et al [8]. This is represented by the following equations:

For the front heat source:

$$q(x,y,z,t)=\frac{6\sqrt{3}f_f Q}{a_1 b c \pi\sqrt{\pi}} e^{-3(x-vt-x_0)^2/a_1^2} e^{-3y^2/b^2} e^{-3z^2/c^2} \quad (1)$$

For the rear heat source:

$$q(x,y,z,t)=\frac{6\sqrt{3}f_r Q}{a_2 b c \pi\sqrt{\pi}} e^{-3(x-vt-x_0)^2/a_2^2} e^{-3y^2/b^2} e^{-3z^2/c^2} \quad (2)$$

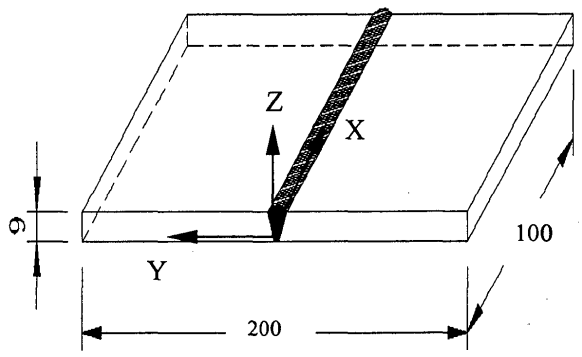

Fig. 1 Geometry of plate and coordinate system.

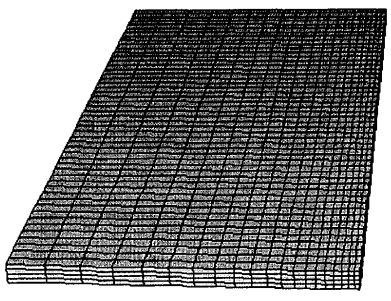

Fig. 2 Plate model used for finite element analysis.

Where, f_f and f_r are parameters which give the fractions of the heat deposited in front and the rear parts, respectively. Note that $f_f + f_r = 2.0$. This is done because the temperature gradient in the front leading part is steeper than that in the tailing edge. Therefore, two ellipsoidal sources are combined, one for the front half and the other for the rear half. Q is the magnitude of the heat input per unit time ($Q=UI\eta$); v is welding speed; t is welding time; and x_0 is the position of the heat source in the x direction when t is zero.

The arc efficiency η, is assumed to be 70% for the TIG welding process. The parameters a_1, a_2, b and c are related to characteristics of the welding arc. In the two equations, the origin of the coordinate system is located at the center of the welding arc, and the coordinate system that is fixed to the weldment. In the finite element model and the Lagrangian formulation of ABAQUS, the welding arc moves in this fixed coordinate system. The parameters of the heat source were adjusted to create the desired melted zone. Another way to determine the parameters of heat source is to make temperature measurements at certain positions and compare these with the computed temperature field and history. The heat source for the moving welding arc is modelled by a user subroutine in ABAQUS.

To consider heat transfer due to fluid flow in the weld pool, an artificially increased thermal conductivity was assumed for temperatures above the melting point. The thermal effects due to solidification of the weld pool were modelled by taking into account the latent heat for fusion. To account for heat losses, both the thermal radiation and heat transfer at the weld surface were assumed.

In order to clarify the effect of phase transformation on welding residual stress and deformation, two kinds of steel, namely low carbon steel (S15C) and medium carbon steel (S45C) were selected in this study. The chemical compositions and thermal properties as functions of temperature are shown in **Table 1** and **Fig. 3**, respectively. In this study, it is assumed that the thermal properties of S15C steel are the same as those of S45C steel.

Table 1 Chemical composition of S15C and S45C steels, wt%.

Steel	C	Si	Mn	P	S	Cr
S15C	0.15	0.22	0.41	0.021	0.024	0.06
S45C	0.44	0.22	0.66	0.022	0.029	0.15

2.2 Phase Transformation

In the present study, a metallurgical analysis based on phase transformation laws [9] was performed to simulate the phase transformation during welding. When a base metal is heated above A_1 (eutectoid temperature)

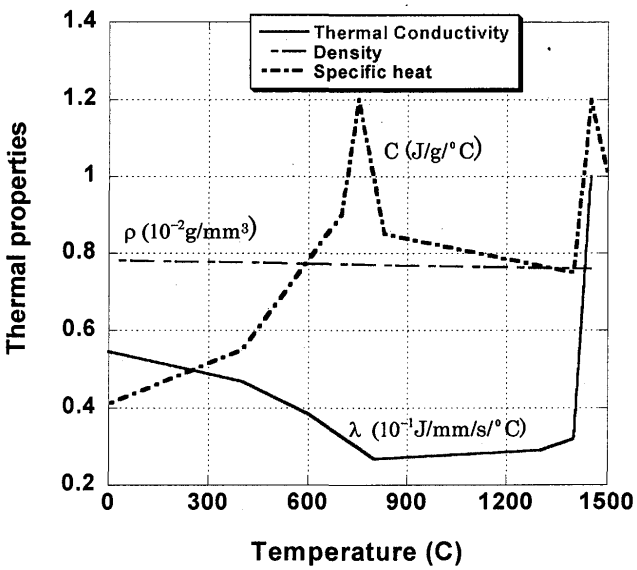

Fig. 3 Temperature dependent thermal physical properties.

temperature, pearlite-ferrite partly transforms into austenite, and when the temperature is higher than A3, pearlite-ferrite completely changes into austenite. For carbon steel and low alloy steel, the A1 and A3 temperatures can be calculated according to the following empirical equations [10].

$$A1 = 723 - 10.7Mn - 16.9Ni + 29Si + 16.9Cr + 290As + 6.4W \quad (3)$$

$$A3 = 912 - 203\sqrt{C} - 15.2Ni + 44.7Si + 104V + 31.5Mo + 13.1W - 30Mn - 11Cr - 20Cu + 700P + 400Al + 120As + 400Ti \quad (4)$$

When the base metal is heated above A1 temperature, the body centered cubic (bcc) structure transforms to the face centered cubic (fcc) structure, and the volume decreases. During rapid cooling, the austenite with fcc structure changes to martensite with a body centered tetragonal (bct) structure, and the volume increases. The volume change due to phase transformation in the course of heating and cooling is schematically shown in **Fig. 4**.

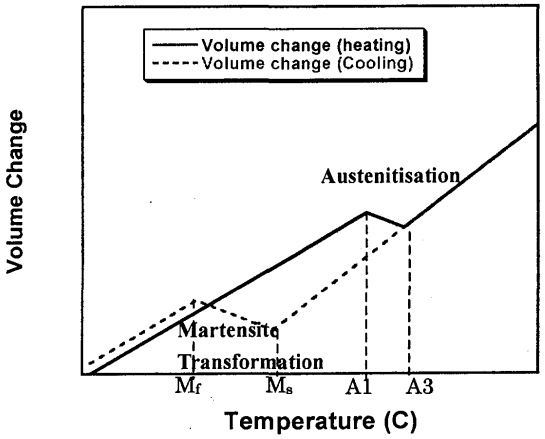

Fig. 4 Schematic diagram of volume change due to phase transformation.

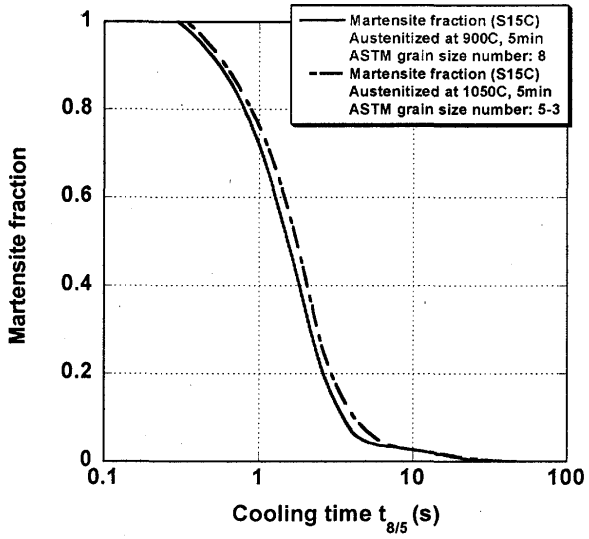

Fig. 5 Martensite fraction as a function of cooling time $t_{8/5}$ for S15C steel.

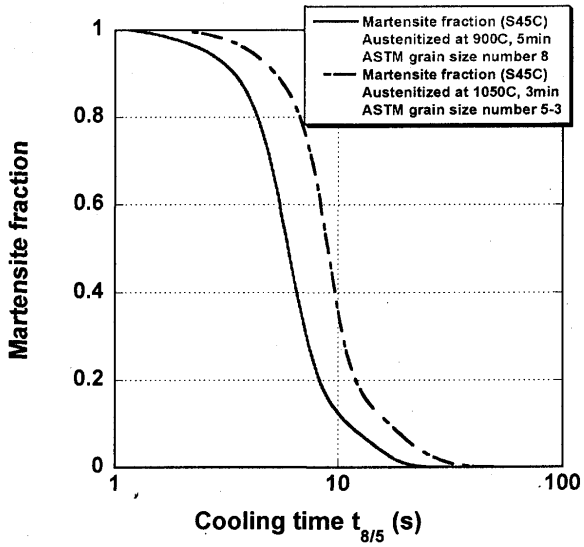

Fig. 6 Martensite fraction as a function of cooling time $t_{8/5}$ for S45C steel.

In this study, depending on the peak temperature that an integration point of an element reached during heating process and the cooling time from 800°C to 500°C, the decision was made whether the point undergoes the martensite transformation or not. From the continuous cooling transformation (CCT) diagram, the relationship between the cooling rate and the fraction of the martensite can be obtained.

In principle, an infinite number of CCT diagrams would be required to describe transformation behavior in every region of the weld metal and the HAZ. Good understanding of the weld transformation behavior can usually be obtained by examining three typical CCT diagrams, namely those for the fine-grained HAZ, the coarse-grained HAZ and the weld metal[11]. The austenization temperature for the coarse-grained HAZ is usually taken in the range 1050-1450°C, and that for fine-grained HAZ and weld metal is A3-1050 °C and 1450°C, respectively. These temperatures take grain growth of austenite into account. Then the decomposition of the austenite into different phases at different cooling rates can be obtained from the cooling curve of the CCT curve corresponding to a particular cooling rate under continuous cooling conditions.

In this study, only the fraction of martensite was predicted using this method. The relationships between $t_{8/5}$ and the fraction of martensite can be obtained from CCT diagrams for S15C steel and S45C steel as shown in **Figs. 5, 6**. Although, the CCT diagram applicable to weld metal has not been prepared by cooling from liquid state, the same CCT diagram was used to predict the fraction of martensite for the fusion zone and the coarse-grained zone in this work. Additionally, the partially transformed zone was neglected.

The CCT diagram in which the austenitizing temperature is 900°C was selected to predict the fraction of martensite for the fine-grained HAZ, and the CCT diagram with austenitization at 1050°C for the coarse-grained HAZ and the fusion zone. The ASTM grain size number is 8 for the fine-grained HAZ, and 5 to 3 for the coarse-grained HAZ and the fusion zone.

On cooling, the martensite transformation was described using the Koistinen-Marburger relationship [3, 9].

$$f_m(T) = f(1-\exp(-b(Ms-T))) \qquad (T \le Ms) \tag{5}$$

Where, f_m is the fraction of martensite at current temperature; T is the current temperature during cooling; and f represents the phase fraction obtained at an infinitely low temperature; and Ms and b characterize initial transformation temperature and evolution of the transformation process according to temperature, respectively.

For carbon steel, the value of constant b is 0.011 [3, 9]. The initial transformation temperature Ms can be calculated using the following equation [8].

$$Ms = 561 - 474C - 33Mn - 17Ni - 17Cr - 21Mo \tag{6}$$

2.3 Mechanical Analysis

The same FE mesh used in thermal analysis was employed here, except for the element type and the boundary conditions. The analysis is conducted using the temperature history calculated by the thermal analysis as the input information. Temperature dependent material properties are taken into account, as shown in **Fig. 7**.

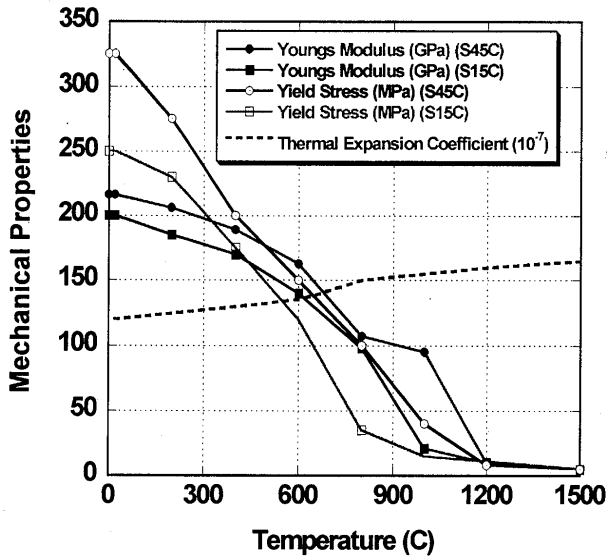

Fig. 7 Temperature dependent mechanical physical properties.

Considering the symmetry of the model and preventing the rigid body motion, the restraint condition as shown in **Fig. 8** is applied.

During the welding process, an additional strain is induced by microstructure evolution during solid-state phase transformation along with the thermal strain. At the same time, transformation induced plasticity is also produced. Therefore, the total strain rate ($\dot{\varepsilon}$) can be written as the sum of the individual components of the strain rate as [4]:

$$\dot{\varepsilon} = \dot{\varepsilon}^{E} + \dot{\varepsilon}^{P} + \dot{\varepsilon}^{T} + \dot{\varepsilon}^{\Delta V} + \dot{\varepsilon}^{Trp} \tag{7}$$

The various components in this equation represent strain rate due to elastic, plastic and thermal loading, volumetric change and transformation plasticity, respectively.

In this study, the volume change was considered, but transformation induced plasticity was not taken into account. Ignoring this component, the strain increment can be written as follows:

$$\Delta\varepsilon = \Delta\varepsilon^{E} + \Delta\varepsilon^{P} + \Delta\varepsilon^{T} + \Delta\varepsilon^{\Delta V} \tag{8}$$

The component $\Delta\varepsilon^{\Delta V}$ is caused by volume change due to phase transformation.

As mentioned previously, the volume of martensite increases, and an additional stress is produced. The strain due to volume change associated with full martensite transformation assigned to the S45C steel and the S15C steel are $\Delta\varepsilon^{\Delta V*} = 8.0\times10^{-3}$ and $\Delta\varepsilon^{\Delta V*} = 2.0\times10^{-3}$, respectively. The volume change due to austenite transformation is assumed to be $\Delta\varepsilon^{\Delta V*} = 2.88\times10^{-3}$ [5].

In principle, when pearlite-ferrite changes into austenite between A1 temperature and A3 temperature, the strain increment due to volume change can be calculated according to the lever law. For the sake of simplicity, a linear relation was assumed in this study. By using the linear approximation, the can be estimated as follows:

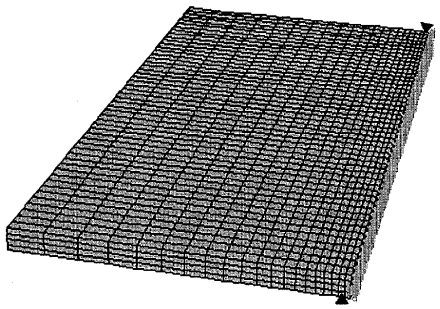

Fig. 8 Boundary condition.

$$\Delta\varepsilon_h^{\Delta V} = -\frac{\Delta T_h}{A3 - A1}\cdot\varepsilon^{\Delta V*} \tag{9}$$

Where, ΔT_h is the temperature increment during heating.

According to the Koistinen-Marburger relationship, the strain increment due to volume change in the course of the martensite transformation process can be determined by the following equation.

$$\Delta\varepsilon_c^{\Delta V} = f\cdot\{-b\cdot\exp[b(T-Ms)\,]\}\cdot\Delta T_c\cdot\Delta\varepsilon^{\Delta V*} \tag{10}$$

Where, ΔT_c is the increment of temperature on cooling. A subroutine to ABAQUS code was developed to compute the fraction of the martensite f and volumetric changes due to martensite transformation.

3. Simulated Cases

To clarify the influence of phase transformation on welding residual stress and deformation, two kinds of steel, namely S15C with a low carbon content and S45C with a medium carbon content were selected. Analyses of residual stress and distortion were performed for the two cases in which phase transformation is considered and ignored. The simulated cases were shown in **Table 2**.

Table 2 Simulated cases.

Case	Material	Heat input	Phase transformation
Case A-1	S15C	450J/mm	No
Case A-2	S15C	450J/mm	Yes
Case B-1	S45C	450J/mm	No
Case B-2	S45C	450J/mm	Yes

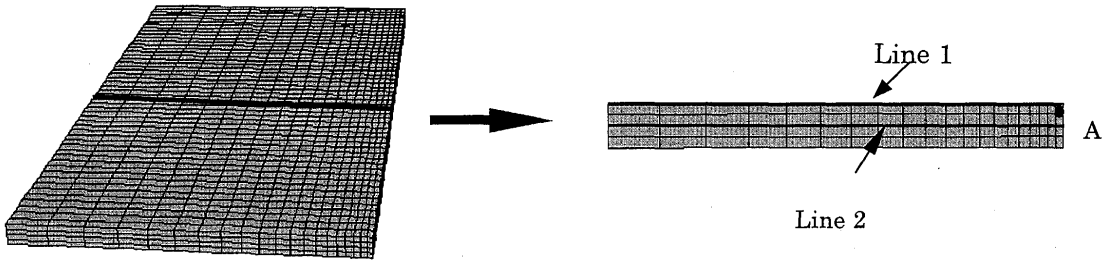

Fig. 9 Middle section of the analysis model.

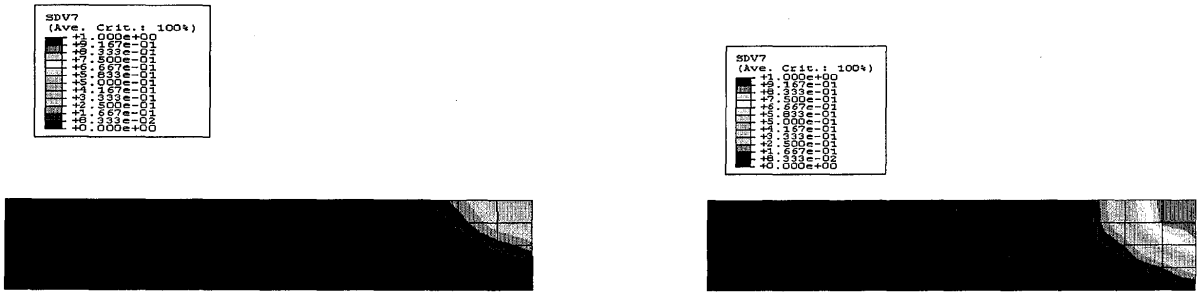

Case A-2 Case B-2

Fig. 10 Martensite distribution in the middle section.

4. Results and Discussion

4.1 Analysis of Residual Stress

In the analyses of residual stress and deformation, both the cases considering phase transformation and ignoring phase transformation were investigated. For the sake of convenience in the following discussion, a middle section of the model was defined as shown in **Fig. 9** and the distribution of the computed values, such as the stress and the deformation, are plotted on this section. In the analyses considering phase transformation, the solid-state phase transformation model described in section 2 was used. **Fig. 10** shows the simulated martensite distributions in the middle section of the model for case A-2 and case B-2 after welding. From this figure, it can be seen that martensite transformation appeared both in Case A-2 and Case B-2. Because the chemical compositions of S15C and S45C are different, the fractions of martensite are different. For steel S45C, the martensite fraction is larger than that of steel S15C because of a relatively high carbon content. **Fig. 11** shows the residual stresses in the welding direction along the line1on the middle section for Case A-1 and case A-2, and **Fig. 12** shows the residual stresses in the welding direction along the line1 for Case B-1 and case B-2.

From Fig. 12, it is clearly seen that there is almost no difference between the case A-1 and case A-2. Because the volume dilation due to phase transformation is relatively small and the transformation temperature is relatively high, phase transformation has little effect on the residual stress. The histories of stress in the welding direction at point A (in Fig. 10) as a function of time for case A-1 and case A-2 are shown in **Fig. 13**. From this figure, a very small decrease in the stress can be seen at the beginning of martensite transformation. When the plate reaches room temperature, a big tensile stress was generated at point A. From the Fig. 12, a compressive residual stress is observed at the centre of welding line in case B-2, in which phase transformation was considered. A clear difference is observed between the residual stresses in Case B-1 and Case B-2. The reason is that the volume dilation due to martensite transformation is very large, and the transformation temperature is relatively low for S45C steel. **Fig. 14** shows the histories of stress in the welding direction for Case B-1 and Case B-2. In the course of heating, a compressive stress is produced in the heated zone. With further heating, the compressive stress is decreased because of the reduction of yield stress with increasing temperature. When the temperature reaches the melting point, the compressive stress is close to zero.

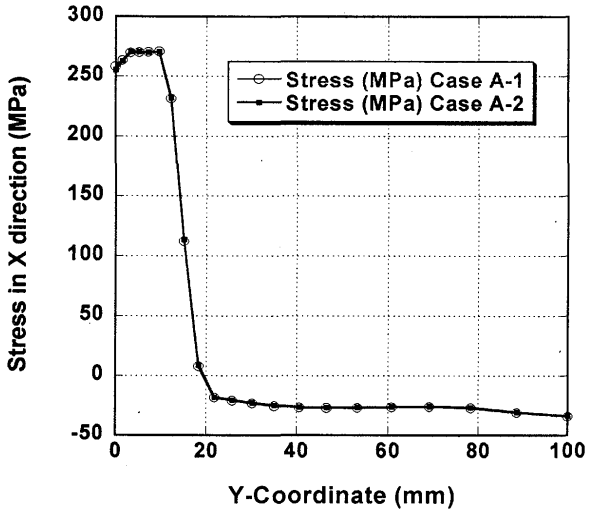

Fig. 11 Residual stress in welding direction of middle section in cases A-1 and A-2.

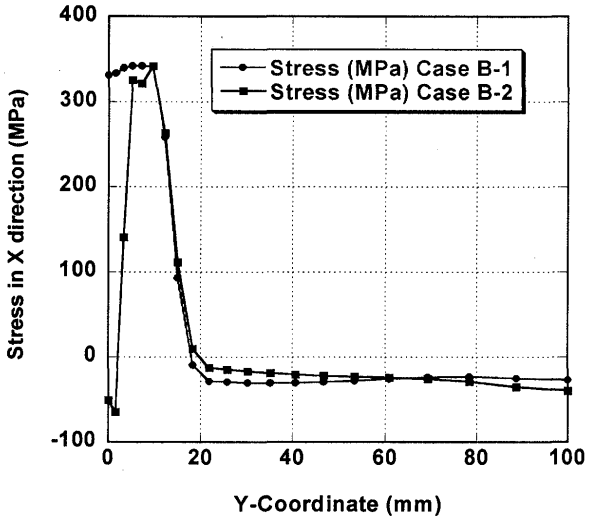

Fig. 12 Residual stress in welding direction of middle section in cases B-1 and B-2.

Upon cooling, a tensile stress in the welding direction is produced because of the shrinkage of the weld. Within the martensite transformation range, a compressive stress is generated again because of a large volume change and the recovery of elastic modulus at a low temperature. After cooling to low temperature, a compressive stress remains in the center of the welding zone. When phase transformation is ignored, a very high tensile stress exists in the center of welding zone as shown in **Fig. 14**. From the results of analysis obtained in this study, it can be concluded that martensite transformation has a significant influence on the welding residual stress for medium carbon steel but small for low carbon steel.

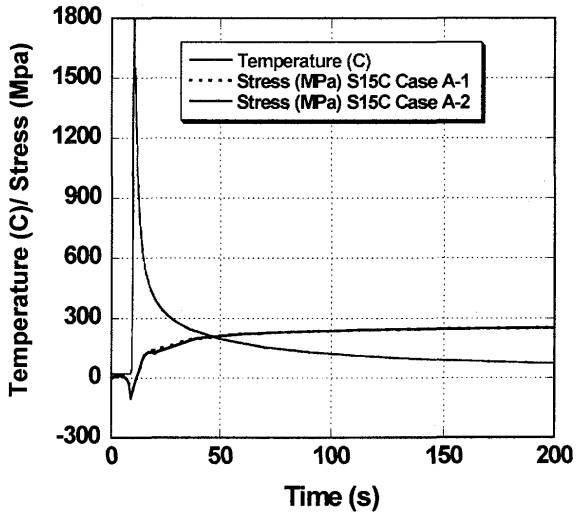

Fig. 13 Stress histories for cases A-1 and A-2 at point A.

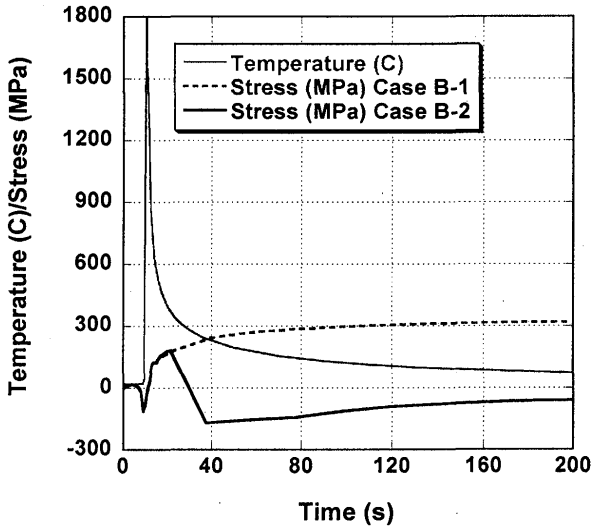

Fig. 14 Stress histories for cases B-1 and B-2 at point A.

4.2 Analysis of Welding Deformation

Fig. 15 shows the vertical deformation in cases A-1 and A-2 along the centerline (line2 in Fig.10) in the middle section of the simulated model. From this figure, it can be seen that there is a small difference between the two cases. **Fig. 16** shows the displacements in the Y direction for cases A-1 and A-2 along the centerline. Similar to the vertical deformation, there is only a small difference between the two cases. From the results of deformation analysis of low carbon steel, phase transformation does not seem to affect the welding distortion.

Fig. 17 shows the vertical deformation of cases B-1 and B-2 along the centerline (lin2 in Fig. 10) in the middle section. It is very clear t hat there is a large difference

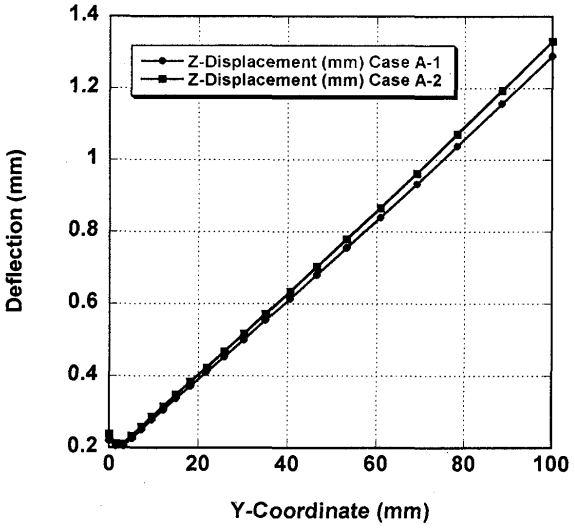

Fig. 15 Deflection along line 2 for cases A-1 and A-2.

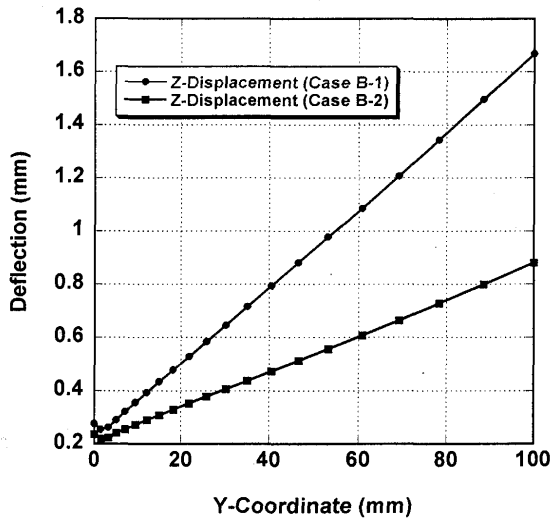

Fig. 17 Deflection along line 2 for cases B-1 and B-2.

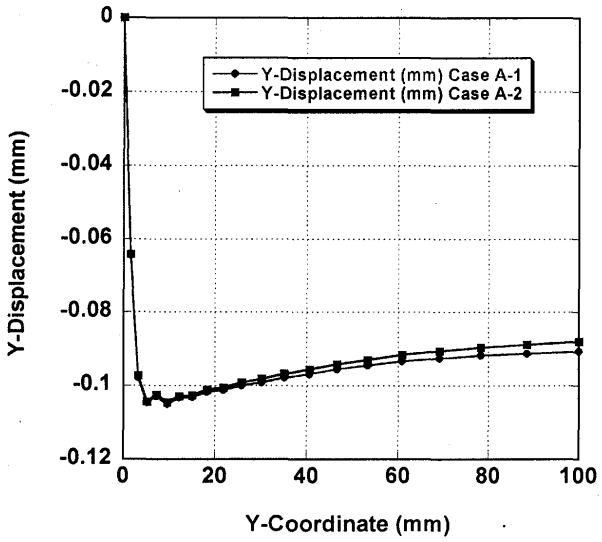

Fig. 16 Y displacement along line 2 for cases A-1 and A-2.

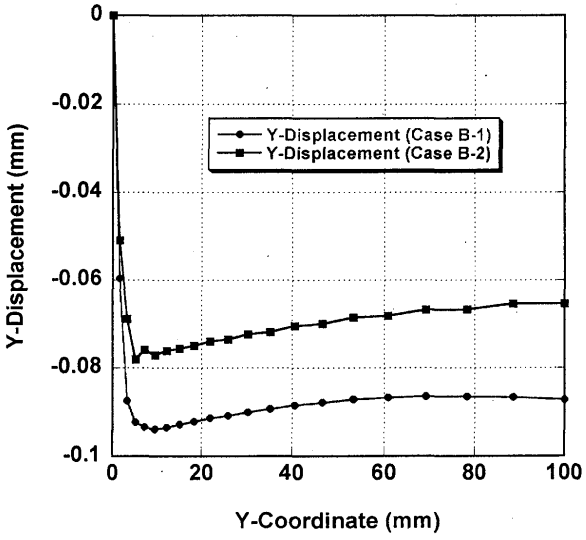

Fig. 18 Y displacement along line 2 for cases A-1 and A-2.

between the two cases. The deflection of case B-2 is smaller than that of case B-1. Because the volume was increased in the course of formation of martensite at a low temperature range, the deflection of case B-2 became smaller. Similar to vertical deflection, a big difference in transverse displacements in the Y direction is observed between Case B-1 and Case B-2 as shown in **Fig. 18**. Because of the dilation induced by a low temperature phase transformation, which partly cancels transverse shrinkage in case B-2, the displacement in the Y direction becomes much smaller than that of case B-1. According to the results, it can be concluded that phase transformation has a significant influence on welding deformation of medium carbon steel.

5. Conclusions

A three-dimensional finite element model considering phase transformation was developed to analyze the tungsten inert gas arc welding process and to simulate the residual stress and the deformation. The proposed method was applied to predict the residual stress and distortion of both low carbon steel and medium carbon steel, and the following conclusions have been drawn.

1. A three dimensional FE model in which solid-state phase transformation was taken into account and effectively applied to the simulation of welding residual stress and deformation.
2. For low carbon steel, phase transformation has an insignificant effect on the welding residual stress and the deformation because of a small dilation due to

martensite transformation and a relatively high transformation temperature range.

3. For medium carbon steel, phase transformation has a significant effect on the welding residual stress and the deformation because of a relatively large dilation and a low transformation temperature range. In this study, it was observed that a compressive stress in the welding direction is produced at the center of the welding zone.
4. As demonstrated by the simulation results, it is necessary to consider solid-state phase transformation in analyses of residual stresses and deformation for medium carbon steel.

References

1) B.Talijiat, B.Radhakrishnan, T.Zacharia, Numerical Analysis of GTA Welding Process with Emphasis on Post-solidification Phase Transformation Effects on Residual Stress, Materials Science & Engineering A 246, 1998, pp45-54.
2) P.Ravi Vishnu, Solid-state transformations in Weldments, ASM Handbook, Vol.6, 1994, pp70-87.
3) George Krauss, Deformation and Fracture in Martensitic Carbon Steels Tempered at Low Temperatures, Metallurgical and Materials Transactions B, Vol.32B, April, 2001, pp205-221.
4) S.Das, U.Chandra, U.Chandra, M.J.Kleinosky and M.L. Tims, Finite Element Modeling of a Single-pass GMA weldment, Modelling of Casting, Welding and Aadvanced Ssolidification Process-VI, 1993, pp593-600.
5) S.H.Cho and J.W. Kim, Analysis of Residual Stress in Carbon Steel Weldment Incorporating Phase Transformations, Science and Technology of Welding and Joining, 2002, Vol.7 No.4, pp212-216.
6) Hibbitt, Karlsson, Sorensen, ABAQUS/Standard User' s Manual, Vol.1,2,3, Version 6.3.
7) S.S Glickstein and E. Friedman, Characterization and Modeling of the Heat Source, ASM Handbook, Vol.6, 1994, pp1141-1146.
8) Goladk.J, Chakravariti A and Bibby M, A New Finite Element Model for Welding Heat Sources, Metallurgical Transactions B, Vol.15, June 1984, pp299-305.
9) D.P. Kosistinen, R.E.Marburger, A General Equation Prescribing Extent of Aaustenite-Martensite Transformation in Pure Fe-C Aalloys and Plain Carbon Steel, Acta Metall. 7 (1959), pp50-60.
10) D.F.Watt, L.Coon, M.Bibby, J.Goldak and C.Henwood, An Algorithm for Modeling Microstructural Development in Weld Heat-affected Zones, (Part A) Reaction kinetics, Acta Metall, Vol 36,No.11, pp3029-3035.
11) G.K.Adil and S.D.Bhole, HAZ Hardness and Microstructure Predictions of Arc Welded Steel-I Review of Predictive Models, Canadian Metallurgical Quarterly, Vol.31, No.2, 1992, pp.151-157.